HYDROLOGICAL PROCESSES
Hydrol. Process. **24**, 2798–2806 (2010)
Published online 28 June 2010 in Wiley Online Library
(wileyonlinelibrary.com) DOI: 10.1002/hyp.7700

Reconstructions of annual discharge and equilibrium line altitude of glaciers at Qilian Shan, northwest China, from 1978 to 2002

Akiko Sakai,[1]* Koji Fujita,[1] Chiyuki Narama,[2] Jumpei Kubota,[2] Masayoshi Nakawo[3] and Tandong Yao[4]

[1] *Graduate School of Environmental Studies, Nagoya University F3-1(200), Nagoya 464-8601, Japan*
[2] *Research Institute for Humanity and Nature, 457-4, Kamigamo-motoyama, Kyoto 603-8047, Japan*
[3] *National Institutes for the Humanities, Tokyo 105-0001, Japan*
[4] *Institute of Tibet Plateau Research, Chinese Academy of Science, Beijing 100085, China*

Abstract:

Discharge was calculated from a mountainous area, including discharge from glaciers, in the Qilian Shan (Qilian Mountains) of northwest China. The studied Yingluoxia basin is 9983 km^2 in area, with glaciers making up 0·3% of the basin. The calculation method was based on the heat balance, requiring only daily temperature and precipitation. Calculated annual discharge from the basin corresponded well with the observed data. Calculated annual discharge from glaciers was 3·6% of the total discharge from the basin.

The temporal trend of the calculated equilibrium line altitude (ELA) at the July 1st Glacier (western side of the Yingluoxia basin) was similar to that of the observed ELA. The calculated annual mass balance of glaciers within the Yingluoxia basin has a larger negative value than the other glaciers in China, as the ratio of accumulation area to the total glacier area in the Yingluoxia basin is much lower than in neighbouring basins to the west. Copyright © 2010 John Wiley & Sons, Ltd.

KEY WORDS discharge; ELA; mass balance; heat balance

Received 11 June 2009; Accepted 18 March 2010

INTRODUCTION

Precipitation is relatively high in the mountainous areas in the arid region of northwest China. Glaciers in mountainous areas store precipitation, acting as a natural reservoir (Fountain and Tangborn, 1985; Jansson *et al*., 2003; Yao *et al*., 2007). Water derived from mountainous areas is an important water resource for the lower parts of the basin, oasis cities and desert areas; consequently, variations in meltwater supply from glaciers have a strong influence on human activity. For example, the Taklimakan Desert contains the ruins of ancient oasis cities (Omar and Takamura, 2001; Yang, 2004) that may have been abandoned because of environmental change related to changes in water resources due to reduced discharge from mountain areas. In this context, the primary aim of this study is to reconstruct historical changes in discharge from the mountainous area of the Hei River basin.

Water discharge from glaciers has been studied by many researchers on the basis of model calculations. For example, Ye *et al*. (1999) and Collins (1987, 2008) investigated long-term variations in discharge, including meltwater from glacial areas in Xinjian, China, and in Switzerland, respectively. Fountain and Tangborn (1985) discussed the relationship between glacier discharge and glacier area, on the basis of annual variations measured in the North Cascade Mountains of Washington State. Braun and Aellen (1990) compared two models that sought to explain observed discharge and the mass balance of the glacier.

In northwest China, Kang *et al*. (1992) evaluated discharge from a glacial area based on observed discharge, calibrated precipitation and estimated evaporation at the Urumqi River in the Tien Shan Mountains. Kang *et al*. (1999) simulated the response of runoff from the Qilian Shan to climate change, using the Hydrologiska Byråns Vattenbalansavdelning (HBV) model. The authors concluded that annual discharge from a mountain area is reduced in the case of annual temperature increases by 0·5 °C and precipitation remains unchanged, as these conditions result in increased evaporation.

Ye *et al*. (2003) calculated the discharge from a glacier in the Tien Shan, China, taking into account temporal changes in the area of the glacier. The authors suggested that the timing of peak discharge depends on the glacier size. Liu *et al*. (2003) reconstructed temporal variations in the areas of glaciers in northwest China since the Little Ice Age, and estimated discharge from the glaciers. However, there are few analyses based on observations of glacier mass balance and discharge for the Qilian Shan. Sakai *et al*. (2009) established a method for calculating

* Correspondence to: Akiko Sakai, Graduate School of Environmental Studies, Nagoya University, Nagoya 464-8601, Japan.
E-mail: shakai@nagoya-u.jp

Copyright © 2010 John Wiley & Sons, Ltd.

discharge from a glacier in the Qilian Shan using only daily temperature and precipitation, on the basis of the heat balance calculation.

The final objective of this research project, to be addressed in a subsequent article, is to reconstruct the annual discharge from the Yingluoxia basin over the past two millennia. As a preliminary study, we applied the above method (Sakai *et al*., 2009) in this article to calculate the discharge from glacier-free areas using meteorological data for recent decades. Moreover, we calculated glacier mass balance near the Yingluoxia basin and investigated equilibrium line altitude (ELA) as validation data.

LOCATIONS AND CHARACTERISTICS OF THE STUDIED BASINS

The Hei River basin, located in northwest China (Figure 1a), can be divided into upper, middle and lower reaches (Figure 1b). The upper reaches consist of three sub-basins (Yingluoxia, Tuolaihe and Hongshuihe basins). The upper reaches are located in the Qilian Shan, which is glaciated. The oasis cities of Zhangye and Jiuquan are located in the middle reaches, at the northern foot of the Qilian Shan. The lower reaches are located in the vast Gobi Desert, where the Hei River enters a terminal lake.

The Hei River basin receives relatively large amounts of precipitation (300–500 mm year^{-1}) in the mountainous zone to the south, but little precipitation (30–50 mm year^{-1}) in the downstream desert area to the north (Wang and Cheng, 1999). Most of the precipitation in the desert zone rapidly evaporates, preventing the accumulation of groundwater and river water; consequently, precipitation stored in mountain glaciers represents an important water resource in such zones (Wang and Cheng, 1999). The Qilian Mountains, including the upper reaches of the Hei River basin, are oriented east–west, with annual precipitation decreasing to the west (Xie *et al*., 1982; Ding and Kang, 1985). The July 1st Glacier is located within the Tuolaihe basin, about 50 km west of the western edge of the Yingluoxia basin. The average annual precipitation and temperature near the glacier terminus (4295 m a.s.l.) are about 350 mm and −6 °C, respectively (Sakai *et al*., 2006b).

From ancient times, the meltwater from glaciers and snow on these mountains has provided water for both drinking and irrigation for those living in oasis cities and desert regions; however, by the latter part of the 19th century, runoff from major tributaries within the Hei River basin had diminished (Wang and Cheng, 1999) because of water extraction for irrigation, thereby altering the environment in the lower reaches of the Hei River basin.

In this article, we focus on the largest drainage area in the upper reaches of the Hei River basin: the Yingluoxia basin. To validate the calculations of glacier mass balance and discharge, we discuss the ELA with reference to the other drainage areas within the upper reaches of the Hei River basin (i.e. the Houngshuihe and Tuolaihe basins) (Figure 1b).

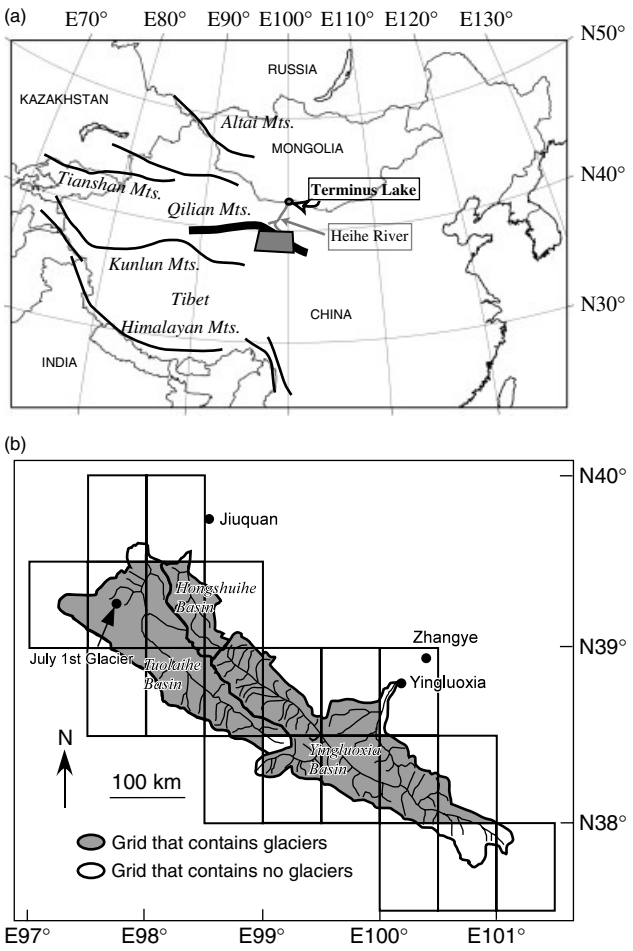

Figure 1. (a) Locations of the Hei River and the Qilian Shan. Thick solid lines represent mountain ranges. The grey area indicates the location of the map shown in (b). (b) Map of the Yingluoxia, Hongshuihe and Tuolaihe basins, located in the upper reaches of the Hei River basin

DATA FOR CALCULATIONS

Distribution of glacier and glacier-free zones

We subdivided the Yingluoxia, Tuolaihe and Hongshuihe basins into two zones (glacier and glacier-free zones) and established a method for calculating the discharge from each zone.

A digital elevation model (DEM) was used to analyse the altitudinal distribution of each basin and the extent of the glacier zone in each basin. The DEM was compiled mainly from Shuttle Radar Topography Mission (SRTM) data, with missing data retrieved from Advanced Spaceborne Thermal Emission and Reflection Radiometer (ASTER) DEM data. The maximum difference in elevation at the boundary between the two DEMs was 5 m.

The boundary of the drainage area was evaluated by superimposing a topographical map (scale of 1 : 100 000) over the ASTER DEM data. The altitudinal distribution of the basin was derived at intervals of 50 m, as shown

Copyright © 2010 John Wiley & Sons, Ltd.

in Figure 2a. The drainage area is 9983 km^2, and 90% of the basin is located at elevations above 3000 m a.s.l.

The glacier zone was extracted by superimposing visible-wavelength LANDSAT5 TM satellite images taken on 3 August 2006 and 13 August 2007, and a DEM produced from an ASTER satellite image. Where possible, we selected LANDSAT satellite images with no clouds or seasonal snow. The altitudinal distribution of the glacier area is shown in Figure 2b. This area accounted for ~0·3% (33 km^2) of the entire basin, and corresponded to elevations between 4200 and 5150 m. Glaciers with an area less than 0·001 km^2 could not be detected from the satellite images.

The altitudinal distributions of glacier and glacier-free areas in the basin were divided into 0·5° grids, as we used daily precipitation created on a 0·5° grid (Xie *et al*., 2007), as described below. Eight of the grids within the Yingluoxia basin and nine of the grids within the Hongshuihe and Tuolaihe basins contain a glacier zone (Figure 1b).

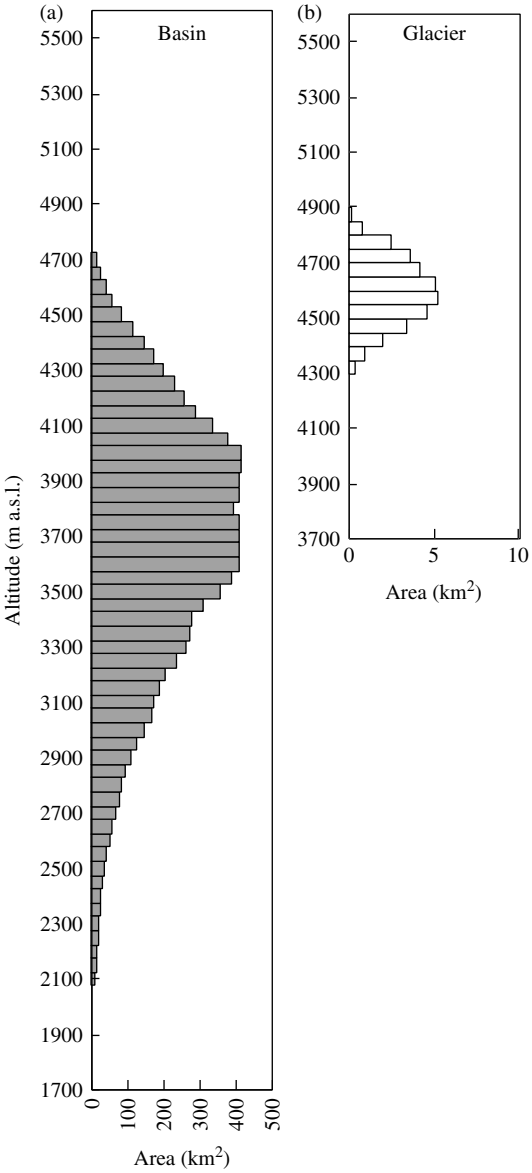

Figure 2. Altitudinal distribution of drainage area (a) and glacier area (b) for the Yingluoxia basin, at altitude intervals of 50 m

Meteorological data

Temperature data at each altitude were estimated from the temperature at 500 hPa [National Centers for Environmental Prediction/National Center for Atmospheric Research (NCEP/NCAR)] assuming a uniform temperature lapse rate. The daily temperature lapse rate was deduced from temperatures between 500 and 600 hPa with geopotential heights. Daily temperatures within the region 37·5–39·5 °N, 98·5–101·5 °E for each 0·5° grid were estimated from the daily temperature at 40°N, 100 °E and 37·5 °N, 100 °E, assuming a linear change in temperature from south to north and assuming that the temperature was uniform from east to west (98·5–101·5 °E). Daily temperatures within the region 38·5–40·0 °N, 97·0–98·5 °E for each 0·5° grid were estimated from the temperature data at 40°N97·5 °E and 37·5 °N97·5 °E.

For the discharge calculation, we used the gauge-based dataset of daily precipitation produced by Xie *et al*. (2007). The dataset was created on 0·5° grids over East Asia for the period from 1978 to 2002. Itano (1997) reported that annual precipitation has a near-linear relation with elevation, but is less dependent on the horizontal location, on the basis of an analysis of observed precipitation from 1988 to 1991 in the mountainous region of the Yingluoxia basin (38°04′N–39°49′N, 99°12′E–101°10′E; altitude: 1310–3200 m).

Figure 3 shows the relation between (1) the difference in annual precipitation reported by Itano (1997) and Xie *et al*. (2007) and (2) the difference in altitude between that observed by Itano (1997) and the average altitude of each 0·5° grid, as deduced from the ETOPO5 dataset

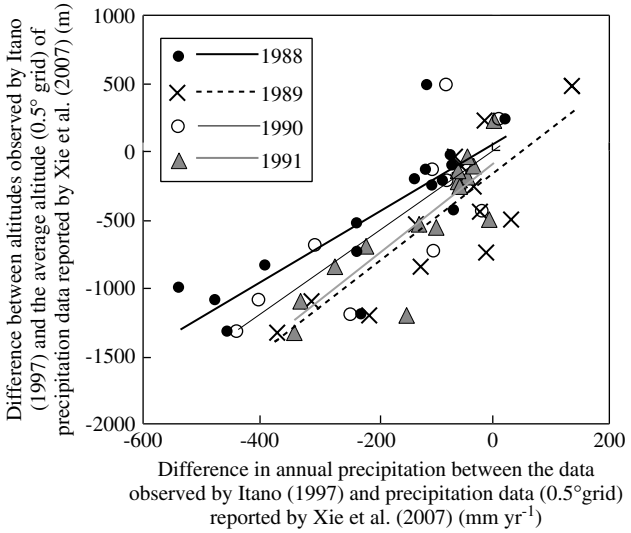

Figure 3. Plot of (1) the difference in annual precipitation between the data observed by Itano (1997) and precipitation data (0·5° grid) reported by Xie *et al*. (2007) versus (2) the difference between altitudes observed by Itano (1997) and the average altitude (0·5° grid) of precipitation data reported by Xie *et al*. (2007)

Copyright © 2010 John Wiley & Sons, Ltd.

produced by National Oceanic and Atmospheric Administration (NOAA's) National Geophysical Data Center (NGDC). The intercepts among the trend lines for each year occur at approximately the zero point on each axis. Therefore, the annual precipitation data produced by Xie *et al*. (2007) are equal to the precipitation at the average elevation of each grid, and the gradients for each year's regression line are approximately equal. On the basis of this result, it is possible to estimate the precipitation at each altitude from the daily precipitation data produced by Xie *et al*. (2007), assuming an altitudinal gradient in precipitation. The gradient of annual precipitation (Figure 3) is approximately equal to the gradient reported by Gao and Yang (1984), based on observed data.

Daily precipitation at z (m) altitude can be estimated from the following equation:

$$P_{\mathrm{r}}(z) = [1 + C(z - z_b)]P_{\mathrm{r}x} \quad (1)$$

where $C = 1/1600\ \mathrm{m}^{-1}$ (Yingluoxia basin) or $1/3360\ \mathrm{m}^{-1}$ (Hongshuihe and Tuolaihe basins), z_b = average altitude of each 0·5° grid, $P_{\mathrm{r}x}$ = daily precipitation data produced by Xie *et al*. (2007).

The constant C is assumed to be uniform throughout each basin. The value of C within the Hongshuihe and Tuolaihe basins was taken from Gao and Yang (1984). The average altitude of each 0·5° grid was calculated from the ETOPO5 dataset produced by NOAA NGDC.

Temporal Changes in Glacier Area

Ye *et al*. (2003) reported that the degree of change in glacier area depends on the glacier size. The South Mountains of the Hexi Corridor are located in the northern part of the Yingluoxia basin. Xie *et al*. (1984) provided data on the area of each glacier and rate of glacier retreat for observed nine glaciers in the South Mountains of the Hexi Corridor. There exists a strong correlation between glacier area and rate of glacier retreat ($n = 9$, $r = -0{\cdot}70$, $p < 0{\cdot}05$) (Figure 4). Hence, we obtained the following equation for the relation between glacier area and the rate of glacier terminus retreat:

$$R_t = -0{\cdot}65A_{\mathrm{g}} - 1{\cdot}68 \quad (2)$$

where R_t is the average rate of the glacier terminus retreat (m year^{-1}), A_{g} is the glacier area (km^2).

The rate of terminus retreat from the 1950s to 1977 for each size of glacier can be estimated from the above equation, assuming that the area of each classified glacier is equal to the median value. We assumed that the rate of glacier retreat from 1978 to 1985 was equal to that from the 1950s to 1977, as the rate of decrease in glacier area was almost constant from the 1950s to 1985 at the July 1st Glacier, with the rate increasing since 1985 (Sakai *et al*., 2006a). Moreover, the retreat rate of glacier termini (at elevations of 4300–4400 m a.s.l.) from 1985 to 2002 was assumed to be the rate from 1975 to 1985 at the July 1st Glacier, as reported by Sakai *et al*. (2006a).

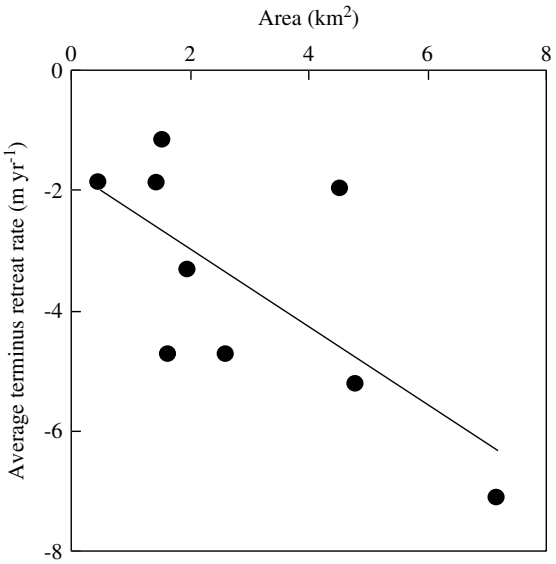

Figure 4. Relationship between the average retreat rate of glacier termini and glacier area for the period 1956–1977 (data source: Xie *et al*., 1984). The regression line is also shown

Data are available regarding the rate of glacier terminus retreat, but the calculation of the glacier mass balance and glacier discharge requires knowledge of temporal fluctuations in the altitudinal distribution of glacier area. Temporal fluctuations were estimated from the rate of glacier terminus retreat, as follows. Each glacier area was classified into one of five size classes (0·001–0·049, 0·050–0·099, 0·100–0·499, 0·500–0·999 and 1·000+ km^2) for each 0·5° grid. Figure 5 shows the frequency distribution of glacier area for the Yingluoxia basin. The average overall altitudinal distribution of glacier areas can be obtained from the altitudinal distribution of each glacier area.

Here, we assumed that the slope of the glacier area is constant, and that the horizontal distance along each glacier is 266 m for a vertical distance of 50 m, corresponding to a glacier slope of 10·646°. We assumed that the altitudinal distribution of glacier area is rhombic in shape (Figure 6), on the basis of the lowest and highest altitudes, the altitude of the maximum glacier area and the glacier area at the altitude of the maximum glacier area, as shown in the figure. These data were derived from the actual altitudinal distribution of glacier area for each glacier size and each 0·5° grid, as mentioned above. Assuming that the rhombus represents the present-day distribution of glacier area, retreat of the glacier terminus was assumed as shown in Figure 6. The altitude of the maximum glacier area was assumed to be fixed; change is only seen in the glacier area at elevations lower than the altitude of the maximum glacier area, as shown in the figure. Thus, the grey area in Figure 6 represents the change in the altitudinal distribution of glacier area in the lower parts of glaciers. We then estimated the change in glacier area from the rate of glacier retreat.

Copyright © 2010 John Wiley & Sons, Ltd.

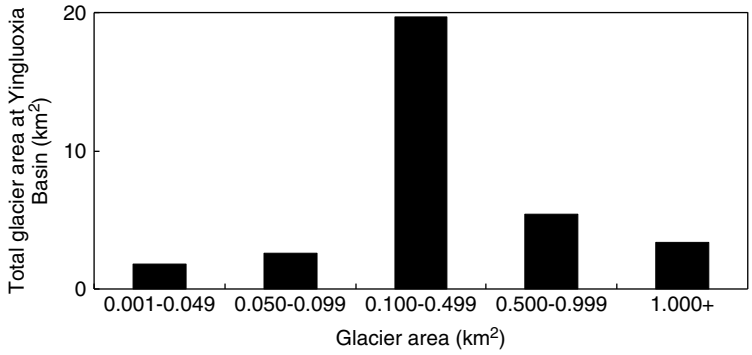

Figure 5. Total glacier area for each size class of glacier area throughout the Yingluoxia basin

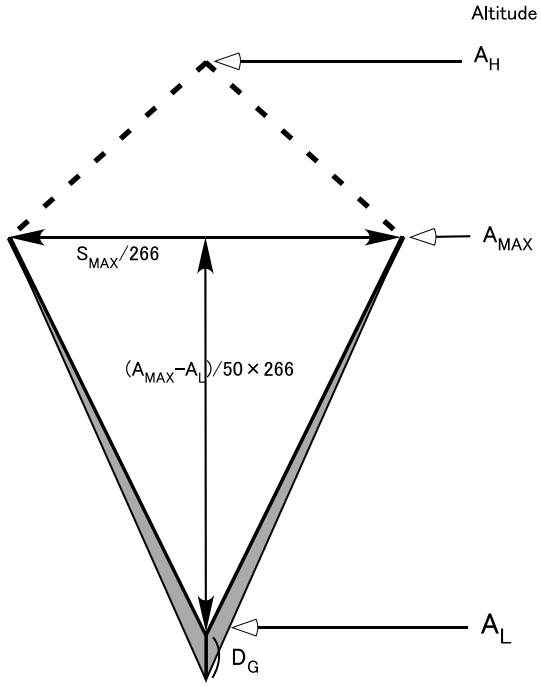

Figure 6. Method employed in calculating the altitudinal change in glacier area based on the glacier terminus retreat. A_H and A_L indicate the highest and lowest altitudes of the glacier area, respectively. A_{MAX} indicates the altitude at which the glacier area is greatest. S_{MAX} indicates the maximum glacier area at the altitude of A_{MAX}. D_G indicates the terminus retreat rate

CALCULATION METHOD

Separation of precipitation

The phase of precipitation, whether solid (snow) or liquid (rain), depends on air temperature. The following relation between the probability of snowfall and air temperature was obtained from data observed by Ueno *et al*. (1994) upon the Tibetan Plateau:

$$\begin{aligned} P_s &= P && [T_a \le 0](^\circ\mathrm{C}) \\ &= \left(1 - \frac{T_a}{6}\right) P_e && [0 < T_a < 6](^\circ\mathrm{C}) \\ &= 0 && [T_a \ge 6](^\circ\mathrm{C}) \end{aligned} \quad (3)$$

and

$$P_r = P_e - P_s. \quad (4)$$

where T_a is the air temperature (°C), P_s is the snow (solid precipitation), P_e is the effective precipitation and P_r is the rain (liquid precipitation).

Here, intercepted precipitation is assumed to be 10% of total precipitation regardless of the phase of precipitation. Then, effective precipitation, P_e, can be calculated as follows:

$$P_e = P_p - P_i, \quad (5)$$

where P_i is the intercepted precipitation ($= 0{\cdot}1\ P_p$) and P_p is the precipitation.

Glacier zone

The positive degree-day (PDD) method is commonly used to estimate the melt rates of glaciers around the world (e.g. Braithwate, 1995; Johannesson *et al*., 1995; Singh *et al*., 2000; Hock, 2003). This method is based on the supposition that rates of ice and snow melt are proportional to air temperature. However, the value of the PDD factor varies widely, depending on the ratio of heat balance elements (i.e. depending not only on latitude and longitude but also on altitude) to total incoming heat, as demonstrated previously (Braithwate, 1995; Johannesson *et al*., 1995; Singh *et al*., 2000; Hock, 2003; Kayastha *et al*., 2003). Subsequently, Sakai *et al*. (2009) developed a method of calculating the glacier mass balance and runoff using only temperature and precipitation data. This method, based on the heat balance calculation, can be used to estimate solar radiation and long-wave radiation from precipitation. Discharge calculated using the PDD method disagrees with observed data, whereas discharge calculated using the method established by Sakai *et al*. (2009) is consistent with observed data.

Mass balance was calculated at intervals of 50 m in altitude. The value of ELA was calculated for the altitude where the total annual mass balance is zero, assuming that the altitudinal profile of annual mass balance shows a linear change.

The following calculations were carried out for each 0·5° grid that contains a glacier zone. Discharge from glaciers and ELA values were calculated for the Yingluoxia basin, whereas only glacier ELAs were calculated for the Tuolaihe and Hongshuihe basins.

Copyright © 2010 John Wiley & Sons, Ltd.

Glacier-free zone

In the same way as calculating glacier melt, the vast difference in the maximum and minimum altitudes within the studied basin (>2500 m) means that the use of an empirical equation to estimate evaporation would lead to a serious misunderstanding of the past hydrological environment in the basin. Therefore, we applied the above method to the glacier-free zone, as follows.

Discharge was calculated as shown in Figure 7. Water flow into the ground at a glacier-free zone can be expressed as follows:

$$W_g = P_r + W_m \tag{6}$$

where W_g is the water flow into the ground and W_m is the meltwater from seasonal snow.

We assume a one-layer bucket at the ground surface; if the amount of water exceeds the maximum storage capacity in soil, the excess flows into the ground and redundant water flows out from the ground.

The final objective of the present study is to reconstruct the 'annual' discharge from the basin for the past two millennia, as stated in the section on Introduction. We can obtain the annual temperature or precipitation data, but not the seasonal change in temperature or precipitation data. Thus, we neglected fluctuations in annual groundwater storage in the studied basin.

In the case of no snow on the ground, we can calculate actual evaporation (E_a) from the ground as follows:

$$E_a = \beta E_p \tag{7}$$

where β is the evaporation ratio and E_p is the potential evaporation.

Here, the evaporation ratio, β, was calculated using the bucket method (Manabe, 1969) as follows:

$$\beta = \frac{w}{w_{max}} \qquad \beta < 1 \tag{8}$$

where w is the soil moisture content at the ground surface and w_{max} is the maximum water storage at the ground surface.

The adjustment parameter for the discharge calculation was the maximum water storage in soil. We adjusted the maximum depth of the bucket so that the average calculated discharge from 1978 to 2002 was similar to the observed value.

Potential evaporation was calculated using the method established by Kondo and Xu (1997a), which defines potential evaporation as evaporation from an ideal water surface, based on the heat balance method and assuming that heat transfer into the ground is zero. The heat balance calculation requires long-wave radiation and humidity, which are difficult to obtain. Therefore, we estimated long-wave radiation and relative humidity from precipitation as the glacier mass balance, calculated according to Sakai *et al*. (2009).

We obtained surface temperature at the ideal water surface by using the method of successive approximation based on the heat balance equation. We then obtained the potential evaporation (Kondo and Xu, 1997a).

In the case of snow on the ground, we assumed no evaporation from the ground surface. Even in the case of snow on the ground, rain penetrates the ground through the snow layer; i.e. we did not take into account refreezing of the seasonal snow layer.

Snow meltwater was calculated using the heat balance method, as follows:

$$H_m = R_n + H_s + H_l + H_g \tag{9}$$

where H_m is the heat available for melting, R_n is the net radiation, H_s is the sensible heat, H_l is the latent heat and H_g is the heat flux into the snow surface.

All components are positive when fluxes are directed toward the surface. Heat flux into the snow surface, H_g, was assumed to be zero.

Net radiation consists of short- and long-wave radiation, as follows:

$$R_n = (1-\alpha)R_s + \varepsilon R_l - \varepsilon\sigma(T_s + 273{\cdot}2)^4 \tag{10}$$

where α is the surface snow albedo (= 0·6), R_s is the downward short-wave radiation (W m^{-2}), R_l is the downward long-wave radiation (W m^{-2}), T_s is the surface temperature (°C), ε is the emissivity of the snow/ice surface (1) and σ is the Stefan–Boltzmann constant ($5{\cdot}67 \times 10^{-8}$ W m^{-2} K^{-4}).

The snow surface albedo was fixed at 0·6, which is the albedo of firn (Paterson, 1994).

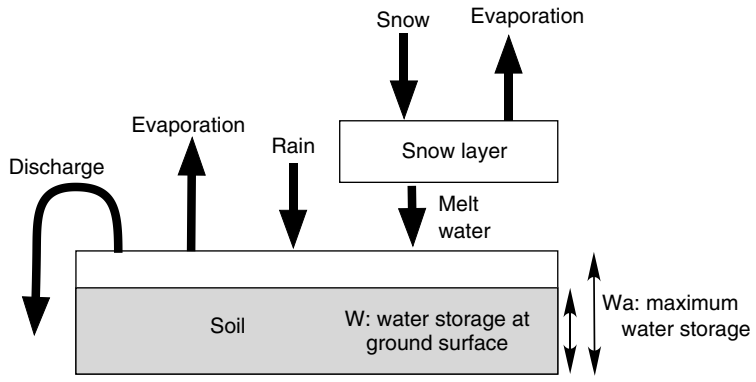

Figure 7. Schematic figure of discharge calculations for glacier-free zones

Copyright © 2010 John Wiley & Sons, Ltd.

Downward long-wave radiation can be estimated from the dew-point temperature at the screen height and a coefficient related to the sunshine ratio (ratio of downward short-wave radiation to solar radiation at the top of the atmosphere) according to the empirical equations of Kondo and Xu (1997b). Their empirical equation was established on the basis of field observations in Japan. Thus, the calculated downward long-wave radiation according to Kondo and Xu (1997b) was multiplied by 0·92 to fit observed data from 2002 to 2005 at the July 1st Glacier. Hence, downward long-wave radiation can be calculated from air temperature, relative humidity and downward short-wave radiation.

Turbulent sensible- and latent-heat fluxes are calculated by the bulk method, as follows:

$$H_s = c_a \rho_a C U (T_a - T_s) \tag{11}$$

$$H_l = l_e \rho_a C U \left[\frac{rh}{100} q(T_a) - q(T_s) \right] \tag{12}$$

where c_a is the specific heat of air [= 1006 (J kg^{-1} K^{-1})], ρ_a is the density of air (kg m^{-3}), C is the bulk coefficient for sensible and latent heat (0·002), U is the wind speed (m s^{-1}), $T_{a,s}$ is the temperature of air ($_a$) and the surface ($_s$), rh is the relative humidity (0–100, saturated at 100), q is the saturated specific humidity (kg kg^{-1}) and l_e is the latent heat for evaporation from the ice surface (2·834 × 10^6 J kg^{-1}).

If we assume that the surface temperature is close to the air temperature, then, $(T_s + 273{\cdot}2)^4 \cong (T_a + 273{\cdot}2)^4 + 4(T_a + 273{\cdot}2)^3 (T_s - T_a)$ and $q(T_s) \cong q(T_a) + \frac{dq}{dT_a}(T_s - T_a)$.

The surface temperature was calculated as follows, from Equations (9)–(12), assuming that heat for melting is zero:

$$T_s = \frac{(1-\alpha) R_s + \varepsilon R_l - \varepsilon \sigma (T_a + 273{\cdot}2)^4 - l_e \rho_a C U \left(1 - \frac{rh}{100}\right) q(T_a)}{4\varepsilon \rho (T_a + 273{\cdot}2)^3 + \left(\frac{dq}{dT_a} l_e + c_a\right) \rho_a C U} + T_a \tag{13}$$

In the case that positive surface temperature is obtained by Equation (13), it is replaced by zero.

Evaporation from the snow surface and snowmelt can then be calculated using the snow surface temperature. In the case that the snow surface temperature is zero, snowmelt occurs and snow meltwater (in water equivalent, W_m) can be calculated as follows:

$$W_m = \frac{H_m}{\rho_w l_f}, \tag{14}$$

where ρ_w is the density of water (1000 kg m^{-3}) and l_f is the specific latent heat for ice melt (0·334 × 10^6 J kg^{-1}).

Change in the amount of snow (in water equivalent) can be calculated as follows:

$$\frac{dl_s}{dt} = P_s - \frac{H_l}{\rho_w l_e} - W_m \tag{15}$$

Discharge from glacier and glacier-free zones was calculated for each 0·5° grid and at 50-m intervals in altitude; the time interval was 1 day.

RESULTS AND DISCUSSION

Figure 8 compares the calculated and observed annual discharge in the Yingluoxia basin. The correlation coefficient is 0·69, indicating the reliability of the reconstructed annual discharge for the basin. The average annual discharge from glaciers accounted for 3·6% of the total discharge from 1978 to 2002. There was no clear increasing (or decreasing) trend in the annual discharge from glaciers over the 23-year period. The proportion of discharge from glaciers is relatively large given that glaciers occupy just 0·33% of the drainage area.

The ELA of glaciers provides validation data for the above calculation, as we calculated not only discharge from glaciers but also the glacier mass balance. Figure 9 shows fluctuations in observed and calculated ELA for the July 1st Glacier (see Figure 1b for the location of the glacier). Both the calculated and observed ELAs are lower in the 1980s compared to 2000, although there are a few observed ELA data.

There occurs an estimation error for precipitation when we calculate the glacier mass balance because there

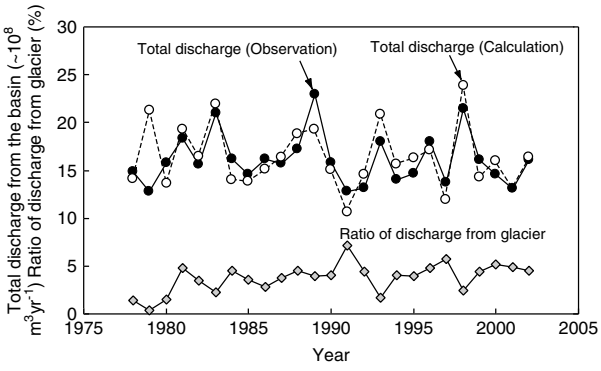

Figure 8. Calculated (white circles) and observed (black circles) annual discharge from the Yingluoxia basin for the period 1978–2002. Grey diamonds show the ratio of calculated discharge from glaciers to the total calculated discharge

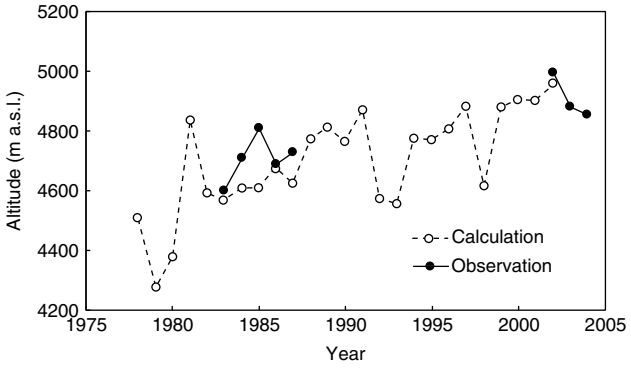

Figure 9. Temporal trend of observed ELA (black circles) at the July 1st Glacier and calculated ELA (white circles) using precipitation data (Xie *et al.*, 2007) at the grid located over the July 1st Glacier

Copyright © 2010 John Wiley & Sons, Ltd.

Table I. Calculated elements for discharge at glacier and glacier-free zones, averaged from 1978 to 2002

Zone	Unit	Precipitation	Discharge	Evaporation	Glacier mass balance
Glacier zone	mm year^{-1} (glacier zone)	565·7	1750·8	203·3	−1388·4
	mm year^{-1} (whole area)	1·9	5·9	0·7	−4·7
Glacier-free zone	mm year^{-1} (glacier-free zone)	338·1	158·7	179·4	—
	mm year^{-1} (whole area)	336·9	158·2	178·8	—
Whole basin	mm year^{-1} (whole area)	338·9	164·1	179·5	−4·7

are few data on the altitudinal trend of precipitation in high mountainous regions in inland Asia. We overcame this problem by using the relation between observed precipitation (Itano, 1997) and the grid data produced by Xie *et al*. (2007) (Figure 3).

Table I lists the calculated elements for the discharge calculation for the entire Yingluoxia basin. Glacier mass loss represents about 80% of the total discharge from glaciers. The average glacier mass balance was −1388 mm year^{-1} for the entire glacier zone, much larger than the values obtained for other glaciers in China; e.g. Urumqi No. 1 (−800 to +200 mm year^{-1} for 1979–2000; Ye *et al*., 2005) and the Xiao (Lesser) Dongkemadi Glacier (−700 to +500 mm year^{-1} for 1988–2001; Pu *et al*., 2008).

Figure 10a shows the east–west distribution of calculated ELA averaged for the period 1978–2002 for each grid over the three basins (Yingluoxia, Houngshuihe and Tuolaihe). Also plotted in the figure is the altitude of the maximum glacier area (AMG) for each grid, which represents the ELA at a time point several decades earlier. It is clear that the calculated ELA is almost equal to AMG for the Hongshuihe and Tuolaihe basins (west side of the Yingluoxia basin), although the calculated ELA is much higher than AMG for the Yingluoxia basin. Figure 10b shows that the east–west distribution of the accumulation area ratio, calculated by glacier area, is higher than the calculated average ELA (1978–2002) relative to total glacier area at each grid. This finding demonstrates that glaciers within the Yingluoxia basin had a large negative mass balance from 1978 to 2002, as the calculated ELA is high compared to the altitudinal distribution of glacier area.

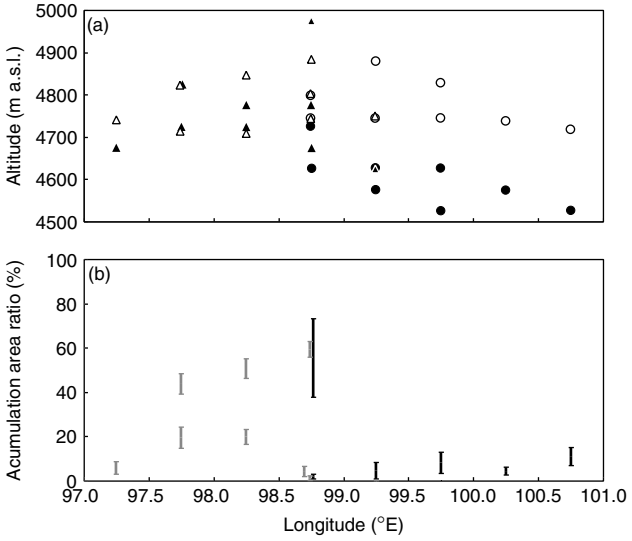

Figure 10. (a) East–west distribution of calculated ELAs (white circles) and the altitude of maximum glacier area (AMG; black circles) within the Yingluoxia basin. White and black triangles show calculated ELAs and AMG for the Hongshuihe and Tuolaihe basins, respectively. (b) Black and grey lines showing the range of accumulation area ratio at each 0·5° grid for the Yingluoxia basin and for the Hongshuihe and Tuolaihe basins combined, respectively

Figure 10b shows that AMGs in the eastern area (i.e. the Yingluoxia basin) are lower than those in the west (Hongshuihe and Tuolaihe basins), although the calculated ELAs are similar in the eastern and western areas. It is possible that the distribution of precipitation has changed in recent decades.

In this study, the altitudinal distribution of precipitation was assumed to be constant, using the relation between observations (Itano, 1997) and the grid database (Xie *et al*., 2007). In future studies, it would be necessary to investigate annual variations in the altitudinal distribution of precipitation in the Yingluoxia basin.

CONCLUSION AND REMARKS

We established a method for calculating annual discharge from a glaciated mountainous area (the Yingluoxia basin) using daily temperature and precipitation data. Temporal fluctuations in the calculated ELA of glaciers are similar to those observed at the July 1st Glacier, located in the Tuolai basin.

The average calculated annual glacier mass balance within the Yingluoxia basin is more strongly negative than that measured for other glaciers in China. The value of ELA (1978–2002) calculated for each grid over the Yingluoxia basin was much higher than the AMG, although the calculated ELA is similar to AMG for the Hongshuihe and Tuolai basins, located west of the Yingluoxia basin. Hence, the accumulation area ratio is very high for the Yingluoxia basin.

Observations of annual change in the altitudinal distribution of precipitation and glacier ELA within the Yingluoxia basin would help in gaining an understanding of the glacier mass balance process in the Yingluoxia basin.

ACKNOWLEDGEMENTS

We thank the staff of the Cold and Arid Regions Environment and Engineering Institute of the Chinese Academy

Copyright © 2010 John Wiley & Sons, Ltd.

of Science in Lanzhou, China, for their generous support during field work. We are also grateful to Prof. Y. Ageta for his valuable suggestions. The field research and data analyses were funded by a Grant-in-Aid for Scientific Research (Project No. 18405002) from the Ministry of Education, Culture, Sports, Science and Technology of Japan (MEXT) and the Sumitomo Foundation. This study was conducted with the assistance of contributions from the Oasis Project (Historical Evolution of Adaptability in an Oasis Region to Water Resource Changes) and the Ili Project (Historical Interactions between the Multi-cultural Societies and the Natural Environment in a Semi-arid Region in Central Eurasia), promoted by the Research Institute for Humanity and Nature (RIHN).

REFERENCES

Braithwate RJ. 1995. Positive degree-day factors for ablation on the Greenland Ice-sheet studied by energy-balance modeling. *Journal of Glaciology* **41**(137): 153–160.

Braun LN, Aellen M. 1990. Modelling discharge of glacierized basins assisted by direct measurements of glacier mass balance. *IAHS Publications* **193**: 99–106.

Collins D. 1987. Climatic fluctuations and discharge from glacierized Alpine basins. *IAHS Publications* **168**: 77–89.

Collins D. 2008. Climatic warming, glacier recession and runoff from Alpine basins after the Little Ice Age maximum. *Annals of Glaciology* **48**: 119–123.

Ding L, Kang X. 1985. Climatic conditions for the development of glacier and their effect on the characteristics of glaciers in Qilian mountains. *Memoirs of Lanzhou Institute of Glaciology and Cryopedology, Chinese Academy of Sciences* **5**: 9–15.

Fountain AG, Tangborn WV. 1985. The effect of glaciers on streamflow variations. *Water Resources Research* **21**(4): 579–586.

Gao Q, Yang X. 1984. The features of interior rivers and feeding of glacial meltwater in the Hexi region, Gansu Province. *Memoirs of Lanzhou Institute of Glaciology and Geocryopedology, Chinese Academy of Sciences* **5**: 131–141.

Hock R. 2003. Temperature index melt modeling on mountain zones. *Journal of Hydrology* **282**: 104–115.

Itano T. 1997. Rainfall over the arid area in the northwestern China: an analysis during HEIFE. *Journal of the Meteorological Society of Japan* **75**: 851–865.

Jansson P, Hock R, Schneider T. 2003. The concept of glacier storage: a review. *Journal of Hydrology* **282**: 116–129.

Johannesson T, Sigurdsson O, Laumann T. 1995. Degree-day glacier mass-balance modeling with applications to glaciers in Iceland, Norway and Greenland. *Journal of Glaciology* **41**(138): 345–358.

Kang E, Cheng G, Lan Y, Jin H. 1999. A model for simulating the response of runoff from the mountainous watersheds of inland river basins in the arid area of northwest China to climatic changes. *Science in China Series D* **42**: 52–63.

Kang E, Yang D, Zhang T, Yang X, Shi Y. 1992. An experimental study of the water and heat balance in the source area of the Urumqi River in the Tien Shan mountains. *Annals of Glaciology* **16**: 55–66.

Kayastha RB, Ageta Y, Nakawo M, Fujita K, Sakai A, Matsuda Y. 2003. Positive degree-day factor for ice ablation on four glaciers in the Nepalese Himalayas and Qinghai-Tibetan Plateau. *Bulletin of Glaciological Research* **20**: 7–14.

Kondo J, Xu J. 1997a. Potential evaporation and climatological wetness index. *Tenki* **44**: 43–51.

Kondo J, Xu J. 1997b. Seasonal variations in the heat and water balances for nonvegetated surfaces. *Journal of Applied Meteorology* **36**: 1676–1695.

Liu S, Sun W, Shen Y, Li G. 2003. Glacier changes since the Little Ice Age maximum in the western Qilian Shan, northwest China, and consequences of glacier discharge for water supply. *Journal of Glaciology* **49**(164): 117–124.

Manabe S. 1969. Climate and the ocean circulation. 1. The atmospheric circulation and the hydrology of the earth's surface. *Monthly Weather Review* **97**(11): 739–774.

Omar G, Takamura H. 2001. Changes in ancient oases and hydrological environment in the southern part of the Taklimakan Desert. 'Land Degradation in the Oases on the South Side of the Taklimakan Desert'. Result Reports of Research Project Grand-in-Aid for Scientific Research (A)(2) 1998–2000. Head Investigation: H. Takamura, Faculty of Geo-Environmental Science, Rissho University.

Paterson WSB. 1994. *The Physics of Glaciers*, 3rd ed. Elsevier: Tarrytown, New York; 480 p.

Pu J, Yao T, Yang M, Tian L, Wang N, Ageta Y, Fujita K. 2008. Rapid decrease of mass balance observed in the Xiao (Lesser) Dongkemadi Glacier, in the central Tibetan Plateau. *Hydrological Processes* **22**: 2953–2958.

Sakai A, Fujita K, Duan K, Pu J, Nakawo M, Yao T. 2006a. Five decades of shrinkage of the July 1st Glacier, Qilian Mountains, China. *Journal of Glaciology* **52**(176): 11–16.

Sakai A, Fujita K, Matsuda Y, Matoba S, Uetake J, Duan K, Pu J, Nakawo M, Yao T. 2006b. Meteorological observation at July 1st Glacier in northwest China from 2002 to 2004. *Bull. Glaciol. Res.* **23**: 23–31.

Sakai A, Fujita K, Nakawo M, Yao T. 2009. Simplification of heat balance calculation and its application to the glacier runoff from the July 1st Glacier in northwest China since the 1930s. *Hydrological Processes* **23**: 585–596. DOI: 10.1002/hyp.7187.

Singh P, Kumar N, Arora M. 2000. Degree-day factors for snow and ice for Dokriani Glacier. *Journal of Hydrology* **235**: 1–11.

Ueno K, Endoh N, Ohata T, Yabuki H, Koike M, Ohta T, Zhang Y. 1994. Characteristics of precipitation distribution in Tanggula, Monsoon, 1993. *Bulletin of Glacier Research* **12**: 39–46.

Wang G, Cheng GD. 1999. Water resource development and its influence on the environment in arid areas of China—the case of the Hei River basin. *Journal of Arid Environments* **43**: 121–131.

Xie W, Kou Y, Zeng Q, Xiao S. 1982. The effect of heat regime of different slopes on accumulation and ablation of glacier. *Memoirs of Lanzhou Institute of Glaciology and Geocryopedology, Chinese Academy of Sciences* **3**: 67–76 (in Chinese).

Xie Z, Wu G, Wang L. 1984. Recent advance and retreat of glaciers in Qilian Mountains. *Memoirs of Lanzhou Institute of Glaciology and Geocryopedology, Chinese Academy of Sciences* **5**: 82–90 (in Chinese).

Xie P, Yatagai A, Chen M, Hayasaka T, Fukushima Y, Liu C, Yang S. 2007. A gauge-based analysis of daily precipitation over East Asia. *Journal of Hydrometeorology* **8**(3): 607–626.

Yang X. 2004. The oases along the Keriya River in the Taklamakan Desert, China, and their evolution since the last glaciation. *Environmental Geology* **41**: 314–320.

Yao T, Pu J, Lu A, Wang Y, Yu W. 2007. Recent glacial retreat and its impact on hydrological processes on the Tibetan Plateau, China, and surrounding regions. *Arctic, Antarctic and Alpine Research* **39**(4): 642–650.

Ye B, Ding Y, Kang E, Li G, Han T. 1999. Response of the snowmelt and glacier discharge to the climate warming-up in the last 40 years in Xinjiang Autonomous Region, China. *Science in China Series D* **42**: 44–51.

Ye B, Ding Y, Liu F, Liu C. 2003. Responses of various-sized alpine glaciers and runoff to climatic change. *Journal of Glaciology* **49**(164): 1–7.

Ye B, Yang D, Jiao K, Han T, Jin Z, Yang H, Li Z. 2005. The Urumqi River source Glacier No. 1, Tianshan, China: changes over the past 45 years. *Geophysical Research Letters* **32**: L21504. DOI: 10.1029/2005GL024178.

Copyright © 2010 John Wiley & Sons, Ltd.